

Rapid Scan White Light Pump-Probe Spectroscopy with 100 kHz Shot-to-Shot Detection

VIVEK N. BHAT^{1,2}, ASHA S. THOMAS^{1,2}, AND VIVEK TIWARI*¹

¹Solid State and Structural Chemistry Unit, Indian Institute of Science, Bengaluru, KA 560012, India

²equal authors

*Corresponding author:vivektiwari@iisc.ac.in

Compiled December 27, 2022

We demonstrate a femtosecond pump-probe spectrometer which utilizes a white light supercontinuum as input, and relies on mutual synchronization of acousto-optical chopper, pump-probe delay stage and the CCD camera to record shot-to-shot pump-probe spectra while the pump-probe delay is scanned synchronously with the laser repetition rate. The unique combination of technologies implemented here allows for electronically controllable and repetition-rate scalable detection throughput that is only limited by the camera frame rate. Despite RMS white-light probe fluctuations of $\sim 5.5\%$, fully leveraging the temporal correlations in white light and fine sampling of pump-probe delay along with 30x reduction in equivalent data collection time compared to stepwise scanning leads to reduction of RMS noise without multichannel referencing down to ~ 0.33 mOD for a scattering nanotube sample. This demonstration opens door for impulsive pump-probe micro-spectroscopy of scattering samples with broadband spectral coverage and minimized sample exposure. © 2022 Optica Publishing Group

<http://dx.doi.org/10.1364/ao.XX.XXXXXX>

Ultrafast transient absorption (TA) spectroscopy has been instrumental in enabling mechanistic insights[1, 2] into condensed phase ultrafast phenomenon ranging from femtosecond charge transfer reactions in solution, energy transfer in excitonically coupled systems such as photosynthetic proteins, and ultrafast exciton diffusion and dissociation in photovoltaic thin films. Although more sophisticated multidimensional spectroscopies[3, 4] are available, the power of TA lies in its relative ease of instrumentation and data processing. TA approaches have also been extended to nonlinear imaging[5, 6] where the additional spatial information has allowed to disentangle the effects of sample morphology on electronic relaxation.

While several TA approaches use a narrowband pump and broadband supercontinuum probe, approaches based on a broadband pump are particularly insightful[2] for inferring structural dynamics accompanying femtosecond internal conversion between electronic states. Although broadband pump

is typically generated through noncollinear optical parametric amplification (NOPA) for reasons of significantly higher RMS stability[7, 8] across the entire bandwidth, white light continuum (WLC) pump is relatively much easier to generate and therefore desirable to implement in TA. However, higher RMS fluctuations in WLC along with spectral and temporal correlations[9] necessitate either longer averaging times, or introducing multichannel referencing and balanced detection[7, 9–11] to achieve desired signal-to-noise (SNR) levels. Alternatively, a few approaches[7] have implemented higher averaging through high-repetition rate shot-to-shot detection, which additionally leverages correlations between consecutive laser shots to suppress laser noise without the complexity of multichannel reference detection. For example, Brixner and co-workers [12] have demonstrated 100 kHz shot-to-shot detection with stepwise scan of pump-probe delay T . It is also known[13, 14] that rapid scanning of T delay can achieve higher averaging through reduction in single scan time. However, in case of WLC sources, it may not by itself be effective in suppressing the low-frequency component of $1/f$ laser noise, which manifests as spectral and temporal correlations[9] in WLC. So far, TA approaches that combine the advantages of rapid scanning with shot-to-shot detection are scarce[7], with limited capability in terms of repetition rate and T scan range. Here we combine the advantages of a broadband WLC source, high-repetition rate shot-to-shot detection and rapid T scanning to demonstrate ~ 30 x reduction in data collection time and noise floor down to 0.33 mOD in femtosecond pump-probe spectra of a scattering nanotube sample. The detection throughput of our approach is electronically tunable and only limited by the camera frame rate, while T delay is sampled densely by scanning synchronously with the laser repetition rate. The particular combination of technologies implemented here makes our approach repetition-rate scalable and especially suitable for high throughput, impulsive pump-probe microscopy with efficient scatter suppression, without added cost and complexity of light sources, multichannel detection or long sample exposure.

The experimental setup schematic is shown in Figure 1 (panel A). Fundamental beam of 1040 nm from a Yb:KGW amplifier (Spirit One) at 100 kHz is split into two arms of ~ 1 μ J pulse energy to generate pump and probe WLC lines. The pump and probe continua are filtered using a 725 nm and 850 nm shortpass filters, respectively. The pump arm is

at each coarse time step already leads to a $\sim 30\times$ slower experiment.

Figure 3 presents the noise analysis of the experiment. Following prior analysis[7], Fig. 3A computes the autocorrelation between 10^5 consecutive probe shots after transmission through the nanotube sample with pump blocked as a function of shot separation j . The closer shots (smaller j) are more correlated. This loss of correlation is better seen as scatter plots (in the insets) for $j = 1$ versus $j = 10$. Panel A suggests strong correlations between consecutive WLC laser shots can be leveraged to bypass multichannel referencing and balanced detection. This is further confirmed in panel B which uses the 10^5 probe shots in panel A to calculate[12] $\Delta OD = \langle -\log_{10} \frac{C_{ON}}{C_{OFF}} \rangle$ for shot-to-shot ($m = 1$) and non shot-to-shot ($m = 10, 100$) schemes. As defined earlier, m is the number of probe shots (with pump ON or OFF) that are averaged together to calculate a difference spectrum, that is, pump-probe spectrum. M is the number of difference spectra recorded for a fixed m . The standard deviation of ΔOD signal (inset), around the expected mean value of zero, is 1.33×10^{-3} for shot-to-shot scheme, which is ~ 1.6 and ~ 3.6 times lesser than the non shot-to-shot schemes ($m = 10, 100$ respectively), suggesting that the advantages of shot-to-shot detection[12] are maintained even in the presence of a scattering sample.

Fig. 3C calculates the average shot-to-shot ΔOD signal for $(s, S) = (1000, 12)$, considering $s - 1$ pairs for averaging with sample present and pump pulse blocked, such that a zero signal is expected. This averaging is the same as that employed for the pump-probe data in Fig. 4. The resulting ΔOD curve is nearly flat (within the error bar) over the entire probe bandwidth suggesting effective averaging of spectral and temporal WLC correlations[9]. The measurement error (gray shaded) ranges from ~ 0.21 - 0.64 mOD. The average RMS error of 0.33 mOD is calculated as $\Delta OD_{RMSE} = \frac{1}{\log(10)} \cdot \frac{\sqrt{(I_i - I_{i+1})^2}}{T}$, where I_i corresponds to i^{th} probe shot and bar denotes average over all possible pairs. ΔOD signal at $T = 1$ ps with pump unblocked is included for comparison. A scaled probe spectrum is also included for reference. Fig. 3D compares this RMS error with the expected shot noise limited calculated as $\Delta OD_{SN} = \frac{1}{\log(10)} \cdot \frac{1}{\sqrt{N_{Ph}}}$ where N_{Ph} is the number of photons falling on the CCD sensor. N_{Ph} can be calculated as $\frac{\text{Pixel Intensity (Counts)}}{\text{max Intensity (for 12bit)}} \cdot \frac{\text{Full Well Capacity}}{\text{Quantum Efficiency}}$, with average quantum efficiency of 0.68 in the probe spectral region, 12 bit resolution and full well capacity of 2.38×10^5 . The individual noise contributions summarized in Table show that $\sim 50\times$ difference between ΔOD_{RMSE} and the shot-noise limit arises from the dominant laser noise in the WLC.

Table 1. Comparison of noise contributions.

	Electronic Noise	Shot noise	Laser intensity fluctuation
mean value	$\bar{C} = 3408$ counts	$N_{Ph} = 2.91 \times 10^5$	$\bar{C} = 3408$ counts
noise	7.7 counts	$\sqrt{N_{Ph}} = 539.6$	187 counts
relative error	2.3×10^{-3}	$\frac{1}{\sqrt{N_{Ph}}} = 1.8 \times 10^{-3}$	54.8×10^{-3}

Using the above described approach, Fig. 4 presents femtosecond pump-probe measurements on a porphyrin nanotube sample. Following previous protocols[16], 1mM meso-Tetra(4-sulfonatophenyl)porphine (TPP) dihydrochloride (Santa Cruz Biotechnology) in Ethanol was added to equal volume of

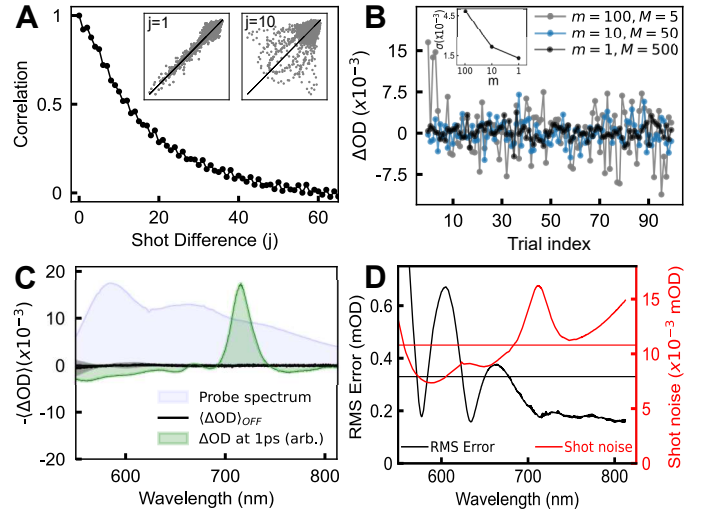


Fig. 3. (A) Laser intensity autocorrelation as a function of shot separation j for 10^5 consecutive probe shots transmitted through the sample with pump blocked, insets: scatter maps for $j = 1$ and $j = 10$. (B) ΔOD calculated with data of panel A assuming data collection schemes. m denotes number of probe shot with pump ON and OFF that lead to one data point. $m = 1$ corresponds to shot-to-shot detection and corresponds to least standard deviation (inset) from the expected zero signal. (C) Average of ΔOD with error bar calculated with the experimental data collection scheme of Fig. 2B but with pump blocked. Green shows ΔOD signal at $T = 1$ ps (with pump ON) on the same scale. Averaged probe spectrum is overlaid for reference. (D) Comparison of RMS Error in ΔOD with the shot noise limit. Horizontal lines indicates the averaged values from 550nm to 812nm region.

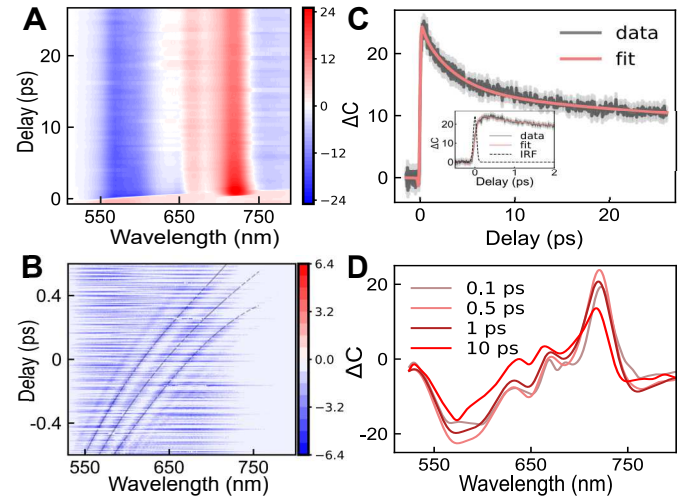


Fig. 4. (A) 2D contour plot of ΔC pump-probe spectra of porphyrin nanotubes. (B) 2D contour plot of the chirp correction signal with the third-order polynomial fit overlaid. (C) Difference signal decay at 720nm overlaid with the error bar and the global fit of the decay. The Gaussian IRF of 95fs FWHM is shown in the inset. (D) Chirp-corrected pump-probe spectra at fixed T .

0.07N HCl/EtOH. Steady state absorption spectrum (Fig. 1B)

confirmed the formation of nanotubes. The pump and probe focal spot sizes at the sample location were measured to be $\sim 25\mu\text{m}$ and $\sim 29\mu\text{m}$ ($1/e^2$), amounting to a pump and probe fluence of 150 and $250\mu\text{J}/\text{cm}^2$, respectively. Over this range of fluence, the measured % transmission of both pump and probe, as well as the pump-probe signal, was confirmed to be linear with pump and probe power. The exciton density was calculated[17] to be 1 per 116 molecules which is lower than the annihilation threshold for the Q band excitons which are delocalized over 88 molecules (when B-Q coupling is neglected)[16].

Fig. 4A is the measured contour map of the pump-probe signal ΔC without probe chirp correction. Although analysis in Fig. 3 considers ΔOD to be consistent with prior reports, we consider changes in probe photon number (ΔC) because it directly relates[18] to the pump-probe signal even if changes in absorption coefficient over the sample pathlength are not small. During setup alignment prior to measurements, any trends in the probe focal spot due to T stage movement were ruled out using a CMOS camera at the focal spot while the stage was continuously moved. Further, probe alignment on the CCD line array was cross verified by scanning the stage in the three scan intervals with the pump blocked. Compared to 5.5% RMS probe fluctuations (Table), maximum deviation in the averaged probe spectra due to T scanning was only 1.9% of the total counts at that pixel. Further, overlapping scan range (of 0.5 ps) were chosen to ensure an overlapping region of ~ 0.5 ps in order to measure and correct for any residual minor deviations during data processing. The data collected in the overlapping regions (denoted by $R = 1, 2, 3$) are compared in terms of the mean over the overlapping region, denoted by $\langle \Delta C \rangle_R$. Minor deviations between different R are then easily corrected by a factor given by the ratio between the overlapping regions. In the measured data, after ensuring the above alignment checks, deviations between $\langle \Delta C \rangle_R$ were found to be of the order of ΔC error bar and easily corrected using the ratio. Chirp correction function is determined by collecting pump scatter and probe interference fringes from an aggregated anthracene solution as a function of T , and fitting the resulting fringes to a third order polynomial (Fig. 4B). The coefficients of this polynomial serve as the initial input for dispersion curve optimization in the GloTarAn[19]. The decay of signal maxima (720 nm) after above corrections is shown in Fig. 4C. A 95 fs IRF suggests significant higher-order dispersion not compensated by chirped mirrors, but may be effectively compensated through liquid crystal or deformable mirror based pulse compressors. It does not however affect the central theme of this report. Pump-probe spectra for representative T points are shown in Fig. 4D. The 2D dataset is interpolated to a uniform delay axis to avoid any loss of signal during chirp correction due to the larger delay steps at later T . From the interpolated data, difference spectra at each T have been sliced along a polynomial corresponding to the dispersion curve, followed by Fourier filtering to eliminate high-frequency noise arising due to interpolation.

Global fitting of the data reveals a tri-exponential decay with ~ 371.5 fs, ~ 3.57 ps, and ~ 95.8 ps decay constants. The faster timescales correspond[20] to intra-Q band electronic relaxation and vibrational relaxation, respectively. The longest decay component of 95.8ps can be attributed to the Q-band exciton lifetime although a ~ 27 ps scan is insufficient to describe it accurately. The positive ΔC signal at 720nm and 670nm correspond

to the Q_x and Q_y bleach signals. The broad excited state absorption (ESA) at 573nm corresponds to transitions to higher excitons while the red-shifted ESA at 765nm corresponds to transitions from the $k \neq 1$ exciton states to multi-excitonic states[20]. The above spectral features and dynamics on TPP nanotubes are in good agreement to the reported literature, with low error bars despite the sample being highly scattering and in continuous flow. While sophisticated double chopping techniques[21] were implemented to suppress the scatter from TPP nanotubes, it should be emphasized that the above data results from a combination of 100 kHz shot-to-shot detection and fine T sampling through rapid scan, without employing any additional scattering suppression techniques. The approach demonstrated here provides a promising path towards high-throughput white-light pump-probe microscopy of scatter prone samples with minimized sample exposure.

Funding. Content in the funding section will be generated entirely from details submitted to Prism. Authors may add placeholder text in the manuscript to assess length, but any text added to this section in the manuscript will be replaced during production and will display official funder names along with any grant numbers provided. If additional details about a funder are required, they may be added to the Acknowledgments, even if this duplicates information in the funding section. See the example below in Acknowledgements.

Acknowledgments. VNB acknowledges research fellowship from DST-Inspire. AST acknowledges Prime Minister's Research Fellowship, MoE India. VT acknowledges the Infosys Young Investigator Fellowship supported by the Infosys Foundation, Bangalore.

Disclosures. The authors declare no conflicts of interest.

Data availability. Data underlying the results presented in this paper are not publicly available at this time but may be obtained from the authors upon reasonable request.

REFERENCES

1. M. Maiuri, M. Garavelli, and G. Cerullo, *J. Am. Chem. Soc.* **142**, 3 (2020).
2. M. Liebel, C. Schnedermann, T. Wende, and P. Kukura, *The J. Phys. Chem. A* **119**, 9506 (2015).
3. F. D. Fuller and J. P. Ogilvie, *Annu. Rev. Phys. Chem.* **66**, 667 (2015).
4. V. Tiwari, *The J. Chem. Phys.* **54**, 230901 (2021).
5. M. C. Fischer, J. W. Wilson, F. E. Robles, and W. S. Warren, *Rev. Sci. Instruments* **87**, 31101 (2016).
6. G. Piland and E. M. Grumstrup, *The J. Phys. Chem. A* **123**, 8709 (2019).
7. B. Lang, *Rev. Sci. Instruments* **89**, 93112 (2018).
8. M. Bradler, P. Baum, and E. Riedle, *Appl. Phys. B* **97**, 561 (2009).
9. M. Bradler and E. Riedle, *J. Opt. Soc. Am. B* **31**, 1465 (2014).
10. A. L. Dobryakov, S. A. Kovalenko, A. Weigel, J. L. Pérez-Lustres, J. Lange, A. Müller, and N. P. Ernsting, *Rev. Sci. Instruments* **81**, 113106 (2010).
11. J. Brazard, L. A. Bizimana, and D. B. Turner, *Rev. Sci. Instruments* **86**, 53106 (2015).
12. F. Kanal, S. Keiber, R. Eck, and T. Brixner, *Opt. Express* **22**, 16965 (2014).
13. J. A. Moon, *Rev. Sci. Instruments* **64**, 1775 (1993).
14. J. W. Wilson and R. A. Bartels, *IEEE J. Sel. Top. Quantum Electron.* **18**, 130 (2012).
15. P. D. Dahlberg, P.-C. Ting, S. C. Massey, M. A. Allodi, E. C. Martin, C. N. Hunter, and G. S. Engel, *Nat. Commun.* **8**, 988 (2017).
16. Y. Wan, A. Stradomska, S. Fong, Z. Guo, R. D. Schaller, G. P. Wiederrecht, J. Knoester, and L. Huang, *The J. Phys. Chem. C* **118**, 24854 (2014).
17. B. Kriete, J. Lüttig, T. Kunsel, P. Malý, T. L. C. Jansen, J. Knoester, T. Brixner, and M. S. Pshenichnikov, *Nat. Commun.* **10**, 4615 (2019).

18. B. Cho, V. Tiwari, R. J. Hill, W. K. Peters, T. L. Courtney, A. P. Spencer, and D. M. Jonas, *The J. Phys. Chem. A* **117**, 6332 (2013).
19. J. J. Snellenburg, S. P. Liptonok, R. Seger, K. M. Mullen, and I. H. M. van Stokkum, *J. Stat. Softw.* **49**, 1 (2012).
20. H. Kano and T. Kobayashi, *The J. Chem. Phys.* **116**, 184 (2002).
21. R. Augulis and D. Zigmantas, *Opt. Express* **19**, 13126 (2011).